Effect of curvature of spherical microscopic indentations on the ellipsometric readout

Daniel Fischer, Michael Griepentrog, Uwe Beck, Matthias Duwe, Jan-Henrik Quast, and Stefan Schneider

Citation: Journal of Vacuum Science & Technology B **37**, 062906 (2019); doi: 10.1116/1.5122252
View online: https://doi.org/10.1116/1.5122252
View Table of Contents: https://avs.scitation.org/toc/jvb/37/6
Published by the American Vacuum Society

Effect of curvature of spherical microscopic indentations on the ellipsometric readout

Daniel Fischer,[1,a)] Michael Griepentrog,[1] Uwe Beck,[1] Matthias Duwe,[2] Jan-Henrik Quast,[2] and Stefan Schneider[2]
[1]*BAM—Bundesanstalt für Materialforschung und -prüfung, Unter den Eichen 44-46, 12203 Berlin, Germany*
[2]*Accurion GmbH, Stresemannstraße 30, 37079 Göttingen, Germany*

(Received 30 July 2019; accepted 16 September 2019; published 8 October 2019)

The authors describe and interpret curvature-related changes to the ellipsometric readout. As model system for a concave curvature, a set of three spherical microscopic indents in silicon (100) of different sizes was prepared by instrumented indentation testing using a spherical indenter. For reference, these samples were characterized by AFM to reveal the topography of each structure. The concavelike indents were analyzed by Mueller-Matrix imaging ellipsometry to extract lateral intensity images of 12 elements of the Mueller-Matrix. As a result of the detailed analysis of the image elements m_{22}, m_{23}, and m_{14}, it was possible to correlate intensity changes and symmetry properties to depolarization and cross polarization induced by the edge threshold and the curved surface of the indent. https://doi.org/10.1116/1.5122252

I. INTRODUCTION

During the last few decades, imaging ellipsometry has shown tremendous potential to analyze topographic surface features on the lateral scale down to the microscopic range.[1,11–14] The obvious advantage of the Mueller-Matrix (MM) imaging technique is the visibility of spatial changes for both depolarizing and nondepolarizing samples. This capability was widely used to detect changes of dielectric properties of the surface, e.g., by adding a thin layer of a different material[2] or detecting residues of adhesives[3] on the surface. In contrast, topographic changes without a spatial polarization contrast—induced by changing the surface material or its dielectric properties—were of minor interest.[4] Recently, it was found that the surface topography alone can result in a lateral contrast in the Mueller-Matrix elements albeit the correlation to structural conditions remains unknown. Thus, a systematic study of different topographic features is necessary and highly symmetrical structures such as spherical caps or indents offer a suitable starting point. In this publication, we provide results on concavelike indents prepared by nanoindentation with a spherical nanoindenter.

II. EXPERIMENTAL DETAILS

Three microscopic concave indents in silicon (100) were manufactured by instrumented indentation testing[5] as shown in Table I. Here, a spherical indenter with a nominal diameter of 5 μm was used to prepare indentations with a spherical concave shape. To adjust the profile of the resulting concave indents, different indentation forces were applied. Subsequently, the profile of each indentation was analyzed by atomic force microscopy (AFM) (*Digital Instruments Dimension 3100*) in tapping mode to reveal the depth and opening diameter of each concavelike indent.

Following the AFM reference measurements, all three indents were analyzed by Mueller-Matrix imaging ellipsometry (MMIE). This measurement technique is described elsewhere[6] in detail. For MMIE, an *Accurion EP4 imaging ellipsometer* with a 50× objective was used to capture 12 image elements of the Mueller-Matrix at an angle of incidence of 50° and 471.0 nm LED light for illumination. The objectives numerical aperture of 0.45 resulted in the respective field of view of 100 × 120 μm^2. Therefore, each detector pixel corresponded to a sample area of 0.15 × 0.33 μm^2.

III. DISCUSSION

A. Indentation topography

The topography of all indentations was analyzed with AFM to reveal the overall shape of the indents for reference. The respective parameters to describe the indentations are the maximum depth, the calotte diameter, which was defined as the edge-to-edge distance on the surface level of each indent, and the roughness. The resulting top-view images of the topography are displayed as insets in Fig. 1. All three samples show a circular shaped indent with different calotte diameters due to the variation of the applied indentation force. For detailed analysis, the profile through the center of the indent was extracted for each sample (Fig. 1). It is clearly visible that indentations (a) and (b) show a significant pileup of displaced substrate material (silicon) on the indentation edges due to the strong forces applied. For indentation (c), this effect was not observed because of the lower indentation force. In general, an increase of the applied force yields deeper and broader indents accompanied by larger amounts of displaced material on the rim. Additionally, a minor increase of roughness (R_q) for decreasing indentation force was found. An overview of the AFM results is given in

Note: This paper is part of the Conference Collection: 8th International Conference on Spectroscopic Ellipsometry 2019, ICSE.
a)Electronic mail: daniel.fischer@bam.de

TABLE I. Results of the AFM reference measurement for all indents.

Indentation number	(a)	(b)	(c)
Indentation force (mN)	187	139	93
Calotte diameter[a] (μm)	4.1	3.5	2.6
Indentation depth (nm)	270	170	40
Roughness,[b] R_q (nm)	8.9	9.9	11.0

[a]The resulting calotte diameter is defined by the edge-to-edge distance in the AFM profile.
[b]The roughness was measured by using a $1 \times 1\,\mu m^2$ square at the center of each indent.

Table I including the comparison of the applied indendation force to the parameters determined by AFM.

B. Mueller-Matrix imaging ellipsometry

1. Readout of the 3 × 4 Mueller-Matrix of curved surfaces

All three curved surfaces were analyzed by measuring the 3×4 Mueller-Matrix (limited to 12 elements due to the ellipsometric setup). For an overview of all possible lateral effects due to polarizing or depolarizing features of each sample, it was necessary to take a deeper look at all experimentally accessible Mueller-Matrix elements. An example of this analysis is given in Fig. 2 for the smallest and flattest indent (c). In this experiment, each pixel represents a measurement of the respective Mueller-Matrix element, and thus lateral changes can be determined by combining all pixels to an image. Due to the oblique angle ($= 50°$), all images show a distortion in the direction of the light path from top to bottom. This results in different pixel dimensions in horizontal ($0.15\,\mu$m) and vertical ($0.33\,\mu$m) directions. The effects we describe, for example, the influence of the curvature, affect each element of the Mueller-Matrix differently, which results in the individual intensity ranges indicated as ΔI in Fig. 2.

By looking into the matrix, it is obvious that the concavelike indent shows a signal in 11 elements ($m_{11} = 1$ by definition[7]). This observation justifies the statement that the indent is not isotropic and has to be depolarized to some degree. Otherwise, the nonblock diagonal elements ($m_{13}, m_{14}, m_{23}, m_{24}, m_{31}, m_{32}$) should be zero and m_{22} should be one.[7] As this behavior is observed over the total measured area of the indent, the depolarization, which is reflected in the ellipsometric readout, must originate in its structural features. This can be verified by comparing with the surrounding silicon (100) area of the indent, where the sample is assumed to be isotropic. Here, the Mueller-Matrix elements show the expected isotropic behavior, i.e., the nonblock diagonal elements are zero. Further, by studying the images in detail, it was observed that all elements show some kind of lateral symmetry illustrating the underlying spherical shape of the concavelike indents as revealed by the AFM reference measurements. However, the lateral symmetry is not identical for all MM-elements, which indicates that further features beyond the curvature of the indent contribute to the ellipsometric response.

To reveal the relevant effects, it is necessary to compare each respective MM-element for all of the three samples and to correlate those results to the topographic properties measured by AFM. For this comparison, the three elements m_{22}, m_{23}, and m_{14} were selected for detailed analyses as they show the most prominent features in the overall MM-images.

2. Detailed analysis: Diagonal element m_{22}

The comparison of the m_{22} images of indents (a)–(c) is shown in Fig. 3 where indentation depth and calotte diameter decrease from top (a) to bottom (c). All three indents provide a significant response. While for an—correctly aligned—isotropic and nondepolarizing sample, the expected response in the m_{22} element would be $I = 1$, and the indents show a deviation from this ideal case.[7] Consequently, depolarization and anisotropy have to be considered. Depolarization effects are expected to play a major role for the investigated samples as the measured sample area is both inhomogeneous and rough according to the AFM measurements. Although the material is isotropic, the curved surface induces cross polarization in the ellipsometric response. Because both, depolarization and cross polarization, result in $m_{22} < 1$, it is assumed that the two effects are superimposed in the m_{22} images.

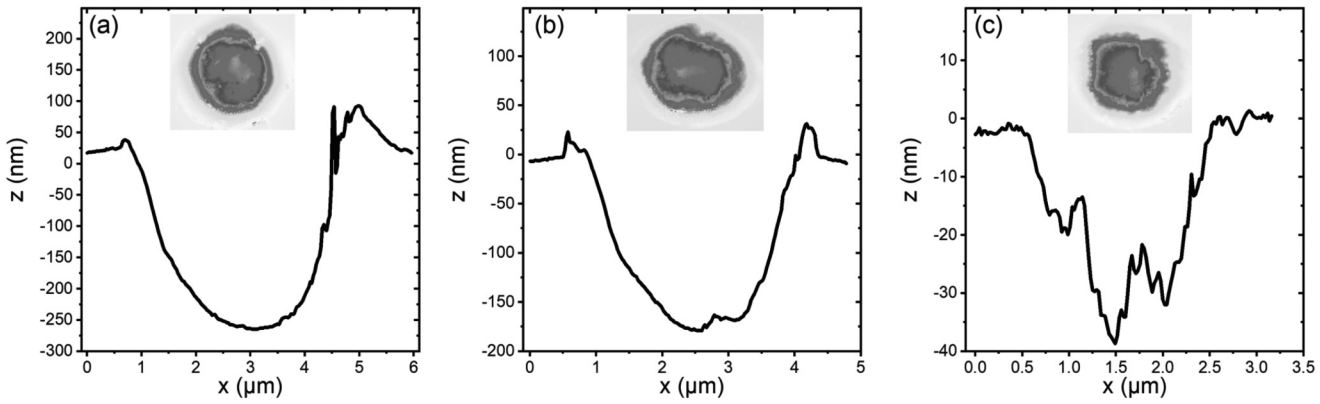

FIG. 1. Topographic top-view images from atomic force microscopy of the indents in silicon (100) as insets and the respective profiles through the horizontal center of the image. Please note the different scaling of the x- and z-axes with micrometer and nanometer.

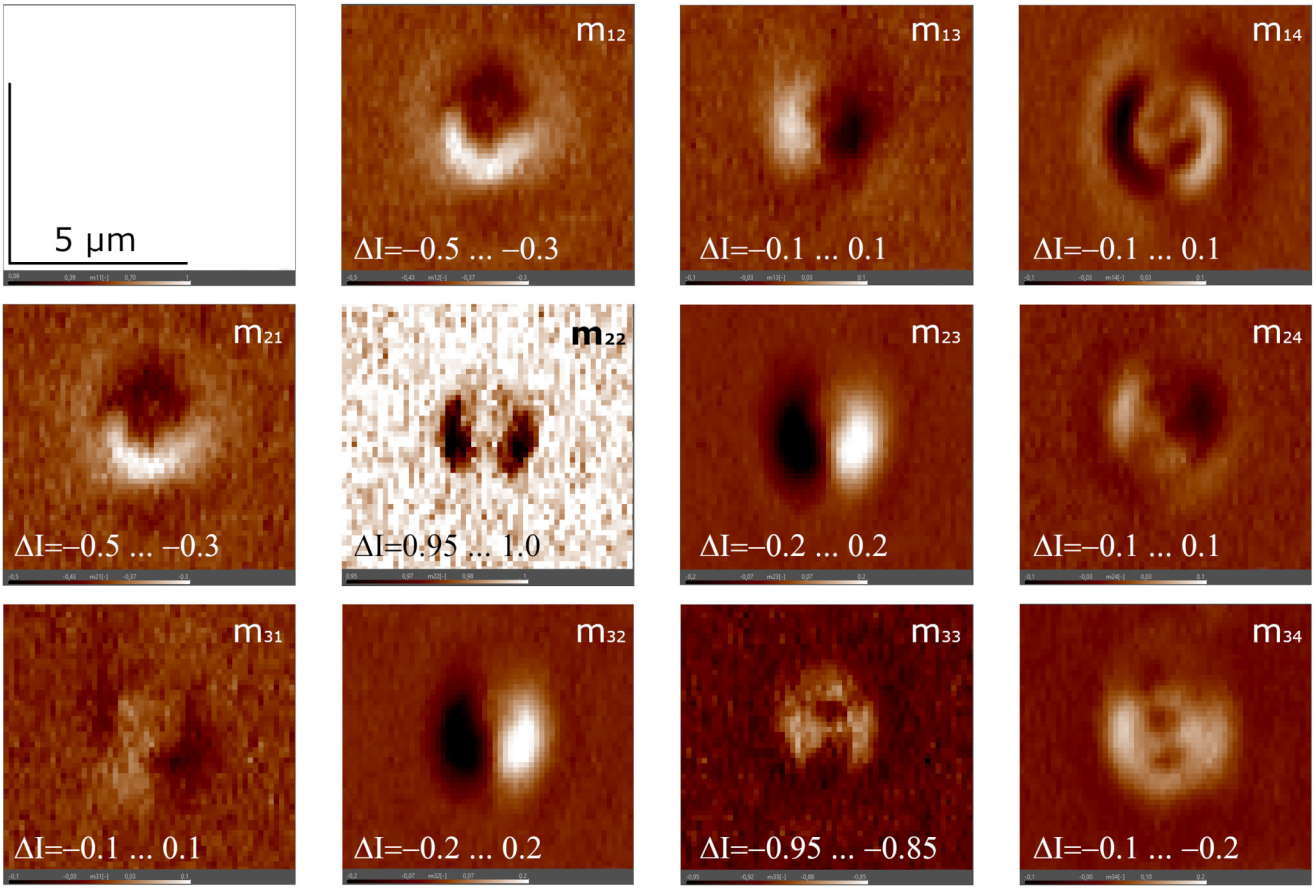

FIG. 2. 3 × 4 Mueller-Matrix of the smallest and flattest indentation [(c); 2.6 μm calotte diameter and 40 nm depth]. The intensity was rescaled individually for each MM-element to improve the visibility of the discussed effects as indicated by ΔI.

Furthermore, in the central cross sections two sharp intensity minima can be identified for all three samples. A quantification of the distance of these minima leads to values of 4.1, 3.4, and 2.6 μm for indents (a), (b), and (c), respectively. These values agree nicely with the opening diameters measured by AFM (4.1, 3.5, and 2.6 μm), which suggests that these minima correspond to the edges of the indentations. Consequently, we can postulate that by analysis of the element m_{22}, the Mueller-Matrix imaging ellipsometry is able to identify realistic dimensions of microscopic indentations. It was also found that the absolute value of the minima is decreasing from indents (a) to (c). This can be correlated to the slope of the indents as shown by AFM [decreasing flatness from indents (a) to (c)]. The possibility of calculating the exact slope and curvature radius has to be evaluated in the future for different curvatures and material compositions. This is particularly interesting as the slope limitations are very low in terms of flatness—the significant intensity minimum for sample (c) can be resolved even though it is already very shallow with an indentation depth of only 40 nm and a calotte diameter of 2.6 μm.

3. Detailed analysis: Off-diagonal element m_{23}

For Mueller-Matrix element m_{23}, which can be found in Fig. 4, the resulting lateral images show a completely different behavior. Here, instead of accentuating the edge region of the indent, the opposite is the case: the edges are blurred, while the inner region of the concavelike indentation is highlighted. Although this Mueller-Matrix element should be zero in the isotropic case,[7] the indents yield clearly visible signals with a prominent lateral symmetry. The signal is centrosymmetric as can be seen in the intensity profile of each indent with the respective quantitative values in Fig. 4. The increased indentation depth and calotte diameter result in a higher intensity signal. The high degree of centrosymmetry in the lateral intensity profile of element m_{23} must be interpreted as the direct result of the indent curvature. Using the center of the indent as the symmetry axis from left to right direction (indicated as white lines in Fig. 4), one can see that the intensity is changing with the same absolute value but opposite signs,

$$I_x = -I_{-x}. \tag{1}$$

This observation leads to the interpretation that the s- and p-polarized part of the reflected light is changing simultaneously depending on the lateral position on the curvature. Considering Eq. (1), the phenomenon is defined as cross polarization.[8] Here, one has direct access to the curvature of the concavelike indent despite interfering factors like roughness are relatively strong [i.e., for indent (c), the roughness is $R_q = 11$ nm at an indentation depth of 40 nm]. Although this

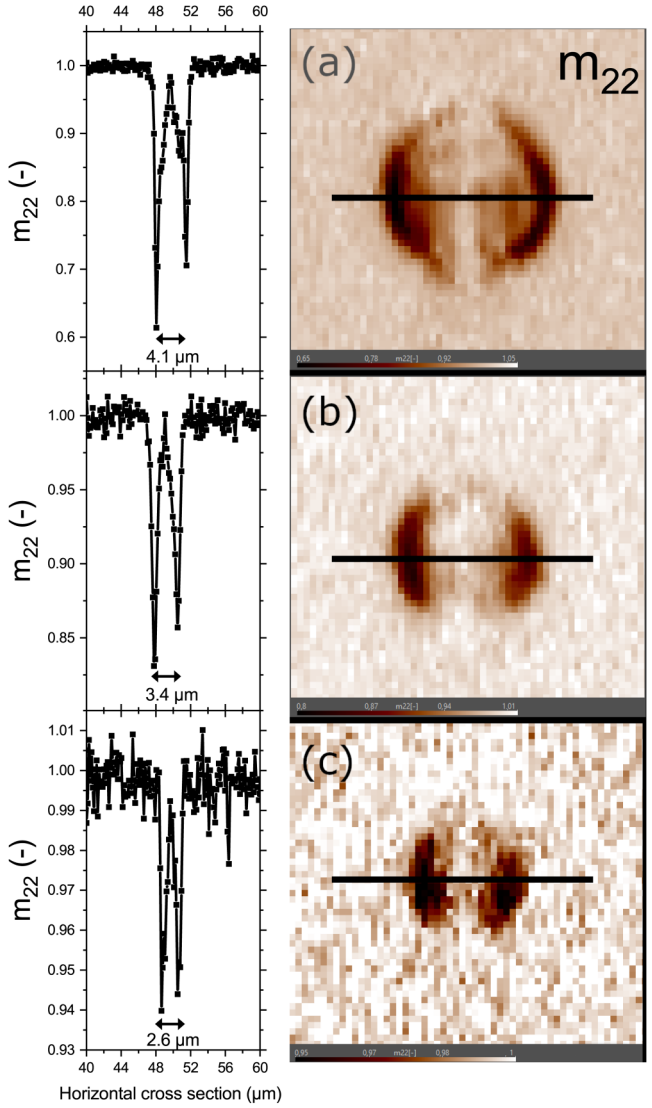

FIG. 3. Lateral intensity profiles of Mueller-Matrix element m_{22} of indentations (a)–(c) and the corresponding images with the position of the profile marked as a horizontal black line. The intensity was rescaled individually for each MM-image to improve the visibility of the discussed effects (refer to the profile for scaling).

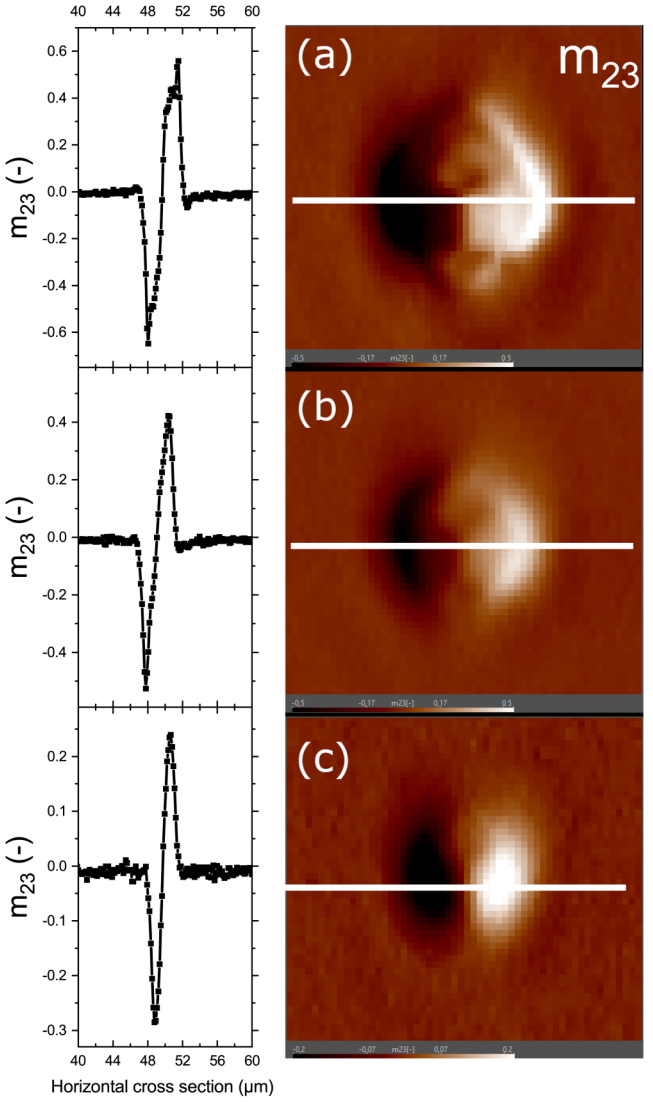

FIG. 4. Lateral intensity profiles of Mueller-Matrix element m_{23} of indentations (a)–(c) and the corresponding images with the position of the profile marked as a horizontal white line. The intensity was rescaled individually for each MM-image to improve the visibility of the discussed effects (refer to the profile for scaling).

publication focuses on the phenomenological description of the effect of concave indents on the Mueller-Matrix, its appearance can be calculated by developing a reasonable mathematical model.[9]

4. Detailed analysis: Off-diagonal element m_{14}

The detailed analysis of the MM-element m_{14} of all three microscopic indents with their respective intensity profiles can be found in Fig. 5. The effects shown there are a combination of the previously found results for m_{22} and m_{23}. As can be seen in the intensity profiles, the edges of the indents show significant signals. However, in contrast to m_{22}, the signals at the edges do not exhibit simple minima, but a structure with an intrinsic centrosymmetry. While this symmetry is clearly detectable for indents (a) and (b), it is barely visible for the flattest indent (c). The observed cross polarization is clearly related to the curvature of the sample surface at the edges. This finding can be confirmed by comparison with the AFM measurements, where a significant pileup of material was found for samples (a) and (b) but none for sample (c). The effect decreases with the flatness of the indent and is correlated to the applied indentation force due to the fact that a higher indentation force results in a bigger pileup. However, by taking a closer look at the m_{14} images one could get a very vivid, almost 3D-like, impression. This effect has a low impact on the intensity profile, but it visualizes an underlying influence on the ellipsometric readout which was not discussed yet. We believe that this barely visible vividness is a representation of the spatial deviation of the evanescent field due to the rapid change of the dielectric contrast on an edge as described by Perin and Hingerl.[10] To prove this interpretation, a study with variously shaped edges is envisioned in the future.

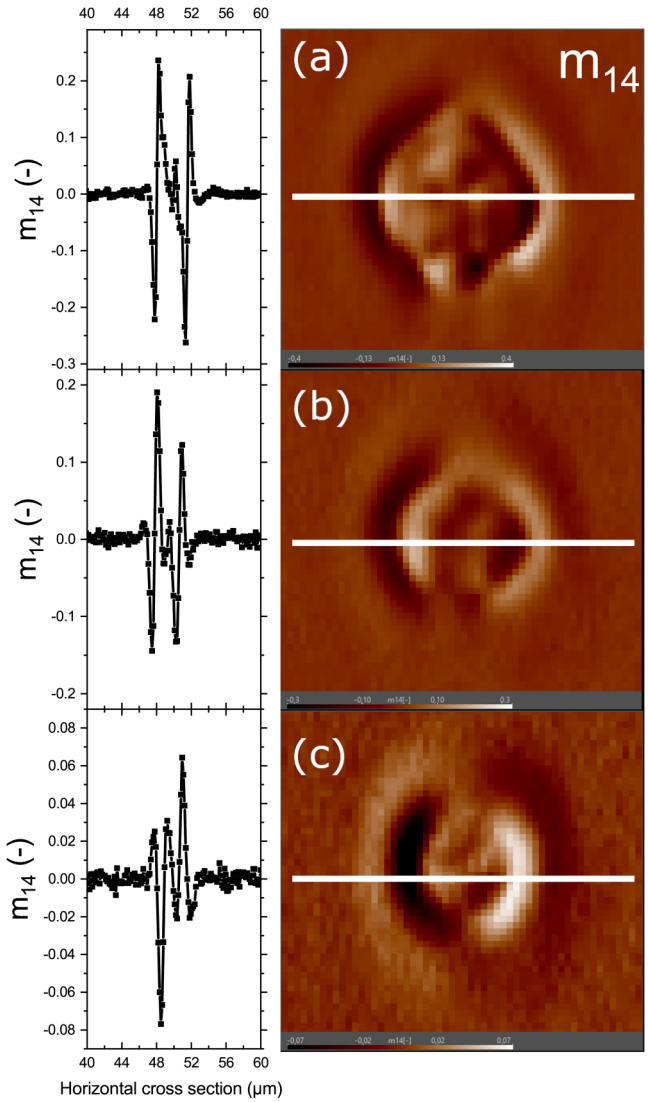

FIG. 5. Lateral intensity profile of Mueller-Matrix element m_{14} of indentations (a)–(c) and the corresponding images with the position of the profile marked as a horizontal white line. The intensity was rescaled individually for each MM-image to improve the visibility of the discussed effects (refer to the profile for scaling).

IV. SUMMARY

It was shown that the Mueller-Matrix imaging ellipsometry is a powerful tool to analyze concave structures. This approach was evaluated by using microscopic concavelike indents in silicon (100) with different sizes as a model system. It was observed that the Mueller-Matrix images contain information about size, structure, and symmetry of the indents. A detailed analysis of the lateral intensity profiles of m_{22}, m_{23}, and m_{14} was performed. It was observed that m_{22} mainly carries information about the edges of the indents due to depolarization effects, while m_{23} contains information about the curvature of the slope, which results in a symmetric cross polarization. Quantitatively, the calotte diameter could be deduced from the lateral m_{22} response, which correlates nicely with AFM reference data. Finally, m_{14} was found to be a combination of both previous effects seen in m_{22} and m_{23}. Additionally, m_{14} offers a vivid, 3D-like image, which could be a representation of the evanescent wave on the edges of the indent as it was theoretically predicted by Perin and Hingerl.[10]

ACKNOWLEDGMENTS

The authors wish to thank Mario Sahre and Sven Grabowski for performing the AFM measurements. The authors gratefully acknowledge the funding for this project from the German Central Innovation Program (AiF-ZIM) with Grant No. ZF4044219AB7.

[1]G. Jin, R. Jansson, and H. Arwin, Rev. Sci. Instrum. **67**, 2930 (1996).
[2]S. Funke, B. Miller, E. Parzinger, P. Thiesen, A. W. Holleitner, and U. Wurstbauer, J. Phys. Condens. Matter **28**, 385301 (2016).
[3]J. Stockmann, A. Hertwig, and U. Beck, Appl. Surf. Sci. **421**, 807 (2017).
[4]W. Q. Li, H. Jiang, C. W. Zhang, X. G. Chen, H. G. Gu, and S. Y. Liu, J. Vac. Sci. Technol. B **34**, 020602 (2016).
[5]ISO 14577-1:2015, *Metallic Materials—Instrumented Indentation Test for Hardness and Materials Parameters—Part 1: Test Method* (International Organization for Standardization, Geneva, Switzerland, 2015).
[6]A. H. Liu, P. C. Wayner, and J. L. Plawsky, Appl. Opt. **33**, 1223 (1994).
[7]R. M. A. Azzam, Proc. SPIE **3121**, 396 (1997).
[8]M. W. Williams, Appl. Opt. **25**, 3616 (1986).
[9]M. Duwe, S. Schneider, D. Fischer, and U. Beck, "Thin-film metrology of tilted and curved surfaces by imaging Mueller-Matrix ellipsometry," J. Vac. Sci. Technol. B (unpublished).
[10]J. P. Perin and K. Hingerl, Appl. Surf. Sci. **421**, 738 (2017).
[11]P. Janicek, S. Funke, P. H. Thiesen, S. Slang, K. Palka, J. Mistrik, M. Grinco, and M. Vlcek, Thin Solid Films **660**, 759 (2018).
[12]G. Jin, P. Tengvall, I. Lundstrom, and H. Arwin, Anal. Biochem. **232**, 69 (1995).
[13]V. Korstgens, J. Wiedersich, R. Meier, J. Perlich, S. V. Roth, R. Gehrke, and P. Muller-Buschbaum, Anal. Bioanal. Chem. **396**, 139 (2010).
[14]S. Y. Liu, W. C. Du, X. G. Chen, H. Jiang, and C. W. Zhang, Opt. Express **23**, 17316 (2015).